Delta Oscillation Coupled Propagating Fast Ripples Precede Epileptiform Discharges

Shennan Weiss (shennanweiss@gmail.com)
SUNY Downstate
Laurent Sheybani
University of Geneva
Nitish Seenarine
SUNY Downstate
Itzhak Fried
University of California Los Angeles
Ashwini Sharan
Thomas Jefferson University Hospital
Chengyuan Wu
Thomas Jefferson University https://orcid.org/0000-0002-3954-2929
Jerome Engel Jr.
UCLA
Michael Sperling
Thomas Jefferson University https://orcid.org/0000-0003-0708-6006
Yuval Nir
Tel Aviv University
Richard Staba
David Geffen School of Medicine UCLA

Article

Keywords:

Posted Date: May 11th, 2022

DOI: https://doi.org/10.21203/rs.3.rs-1640013/v1

Abstract

Epilepsy can be considered a network disorder in which distinct and sometimes widespread brain regions coordinate their activity to generate seizures. Fast ripples (200-600 Hz) are associated with epileptogenic brain tissue and play critical roles in the epileptic network. Using macroelectrode stereo EEG recordings from a cohort of 46 patients we found that propagating fast ripples exhibited a distinct frequency and larger power ($p<1e-4$) and were strongly phase coupled to the peak of delta oscillation DOWN states during non-REM sleep ($p<1e-10$). Fast ripple propagation in the seizure onset zone often was followed by an epileptiform spike ($p<0.05$). Thus, under the premise that GABA-mediated depolarizing potentials generate fast ripples, our results indicate that fast ripple propagation is representative of increased neuronal recruitment of pathologically interconnected neurons overcoming surround inhibition to activate neighboring pathologic neurons and promote epileptiform discharges. These results support the epileptic network and inhibitory restraint hypotheses of seizure genesis.

Introduction

Epilepsy affects 1% of the population and is associated with significant morbidity and mortality. One third of patients with focal epilepsy are drug resistant and are potential surgical candidates[1]. Spontaneous epileptic seizures can arise from coordinated activity between local or widespread brain regions, which can be conceptualized as nodes in a network[2]. The epileptic network hypothesis is supported by a plethora of structural[3] and functional neuroimaging, and EEG/MEG evidence[2,4,5]. Despite the clinical correlations supporting the network hypothesis, how network activity generates seizures is unknown.

The mechanisms generating seizures are diverse and could involve a pathologically large synaptic excitatory drive overcoming a restraint from synaptic inhibition[6,7]. Fast ripples (FR) are high-frequency (200–600 Hz), brief bursts of spectral energy in the EEG closely linked to injury provoked epileptogenesis. FR are believed to correspond with predominately excitatory discharges generated by clusters of pathologically interconnected neurons (PIN) as small as 1 mm[8,9]. In patients, FR have been found to both partially coincide with epileptogenic lesions and the seizure onset zone (SOZ), and when FR occur outside these regions, failure to resect a sizable proportion of the FR generating sites has been shown to correlate with a recurrence of seizures[10]. One explanation is residual FR generate seizures. Supporting this hypothesis is evidence that shows for some focal seizures FR of incrementally increasing power precede the onset of ictal discharge[11] as this may relate to the FR network related state change overcoming an inhibitory restraint mechanism that may ordinarily curtail the generation of spikes and seizures[6,7]

Since FR produced by PIN clusters appear to be critical to epileptogenesis and seizure genesis it is plausible the networks of the temporal correlations of FR could be insightful and may be representative of actual pathological interactions in the epileptic network. We recently found that in patients who underwent epilepsy surgery and had no improvement in seizure frequency or severity, or in patients with

widespread seizures who were not deemed surgical candidates, FR can arrange in a decentralized widespread network where individual sites are highly active though relatively desynchronized[12]. Whether the FR temporal correlations in these networks are epiphenomenon related to internal or external inputs, or whether the FR events actively propagate from one brain region to another as a form of direct communication between nodes of the network is unclear[13]. We use the term 'FR propagation' throughout the manuscript, since we believe this is the most likely interpretation supported by the data (presented and discussed below), but we acknowledge from the outset that time lags observed in FR occurrence may also reflect a common synaptic driver to nodes that do not necessarily communicate directly.

To investigate whether the temporal correlations of FR events underlie epileptic networks, we tested if unidirectional FR propagation occurrences require a distinct neurophysiological context and are associated with macroscopic neurophysiological changes in the broad band intracranial EEG (iEEG) during non-rapid eye movement (REM) sleep. Such associations could imply that the FR propagating events alter the pathological network's excitability through a state change that occurs during, but is independent from, the UP-DOWN or DOWN-UP transition[14]. We were particularly interested whether FR propagation would be associated with the generation of epileptiform spikes as this may relate to the FR network related state change overcoming an inhibitory restraint mechanism that may ordinarily curtail the generation of spikes and seizures[6,7].

Results

We identified and characterized FR during non-REM sleep (Figure S1) in a cohort of 46 patients implanted with stereo-EEG (SEEG), which was required for pre-surgical evaluation. The focality of the patients' seizures varied, as did the surgical interventions, and the patients' post-operative seizure outcomes (Table S1). We examined the temporal dynamics and interactions of FR generating sites to understand the mechanisms that underlie FR networks and to relate them to interictal spikes and sharp waves.

Characterizing fast ripple propagation

For each patient we compared FR onset times between each pair of electrode contacts (*i.e.*, nodes) to determine which pairs exhibited unidirectional statistically significant FR propagation (*i.e.*, edges; sign test, $p < 0.005$, FDR corrected, see methods). We excluded FR that coincided with epileptiform spikes, which occur during inter-ictal[15] and ictal epochs[11]. Overall, per patient, FR propagation was rare, and correlated with the mean number of FR per electrode contact ($R^2 = 0.435, 0.105$, $p < 0.05$, Figure S2A). In the SOZ (*i.e.*, SOZ:SOZ), 0.86% ± 0.33% of edges (n = 29) with FR mutual information (MI) greater than zero had statistically significant propagation. In the non-SOZ (*i.e.*, NSOZ:NSOZ), 0.24% ± 0.13% (n = 25) of edges had significant propagation (Kruskal Wallis d.f.=1, $X^2 = 0.01$, $p > 0.05$). In the SOZ:NSOZ (or NSOZ:SOZ), 0.064% ± .18% of the edges (n = 11) had propagation. Visual inspection confirmed FR propagation for significant SOZ:SOZ edges and demonstrated that at the out-node (*i.e.*, FR origin), and sometimes also the in-node (*i.e.*, FR destination), FR precede epileptiform spikes and sharp waves

(Fig. 1A,S3A,S7A). For NSOZ:NSOZ, NSOZ:SOZ, and SOZ:NSOZ edges with significant FR propagation, visual inspection was confirmatory but the associated events in the broadband intracranial EEG were diverse (Fig. 1B, S4, S5, S6 S7B). For SOZ:SOZ edges we found a mean FR propagation velocity of 1.54 mm/sec[13], but velocities across edges varied more than previously reported[13] (Fig. 1C). FR Propagation in the NSOZ:NSOZ, SOZ:NSOZ, and NSOZ:SOZ edges was at a slower velocity than the SOZ:SOZ edges (Fig. 1C). The neuroanatomical location of the edges showing propagating FRs were most often in limbic and frontal regions (Fig. 1D,S2C).

To assess whether FR propagation results from a common synaptic driver inducing responses at the in- and out-node near-simultaneously, we compared the spectral frequency, duration, and power of each FR event. We assumed that if this driver was responsible for the measured pseudo-propagation the properties of the propagating FR events at the in- and out-node should be similar. We defined propagating FR as FR in either the in- or out-node that coincide with a FR in its paired node by < 250 ms in edges with significant propagation. For predicting FR frequency, the four-way interaction of whether the node was out- or in- relative to the propagation direction (*i.e.*, node status), if the FR was propagating (*i.e.*, propagation status), the mean delay of propagation, and whether the contact detecting the fast ripple was in the seizure onset zone (*i.e.*, SOZ status) was significant (generalized linear mixed effects model, GLMM, $p < 1e\text{-}4$, Table S2). Only in the SOZ:SOZ edges did edges with a relatively shorter propagation delay and propagation distance exhibit lower FR frequencies when they were non-propagating FR events in the out-node (Fig. 2A). This suggests that the FR propagation was not due to volume conduction. Power was predicted by the three-way interaction of the node status, propagation status, and SOZ status (GLMM, $p < 1e\text{-}4$, Table S3) and propagated events at the out-node were highest in power (Fig. 2B). Furthermore, the propagating FR power at the out-node was largest at longer propagation delays and propagation distances (GLMM, $p < 1e\text{-}3$, Table S3, Fig. 2B3). Therefore, because of the distinct frequency and power of the propagating FR in the out-node, it is more likely that FR propagate through slow and likely polysynaptic mechanisms to the in-node as opposed to pseudo-propagation from a common driver. Notably, pseudo-propagation could have resulted in differences in FR properties in the out and in node, and even differences in “propagating” events due to variation in the neuronal elements influenced by the driver, but pseudo-propagation cannot easily account for the interaction of node status and propagation status, and the correlation of propagation delay with FR frequency and power. In the case of NSOZ:NSOZ, NSOZ:SOZ, and SOZ:NSOZ edges, the differences in FR frequency (Fig. 2A2,3) and FR duration (GLMM Table S4, Fig S8) for propagating and non-propagating FR events in the in- and out-node were distinct from the SOZ:SOZ edges, suggesting different mechanisms.

Delta oscillation and fast ripple coupling and propagation

Although the FR properties analysis support FR propagation, a synaptic driver to FR generating nodes has been found in studies of the kainic acid model of mesial temporal lobe epilepsy[16,17]. Delta oscillations (3–5 Hz) have been shown to entrain multi-unit activity and FR during the peak of the wave[16,17]. We found in patients, nodes with FR coupled to delta at or around the peak were common in the SOZ

(Rayleigh Z, $p < 0.001$; Fig. 3A,B1). In the NSOZ, delta coupling occurred at more diverse preferred phase angles (Fig. 3B2). To relate the FR-Delta coupling to propagation we predicted the sign test Z value (*i.e.* the propagation significance measure) with the interaction of out- and in-node FR-delta coupling strength (*i.e.*, Rayleigh Z value the phase locking strength measure), and the relative location of the nodes in the SOZ or NSOZ (GLMM, $p < 1e\text{-}9$, Table S5). In this model, the predictive power of delta coupling in the out-node was greater than the in-node (Table S5). The SOZ:SOZ edges with FR-delta coupling in both the out- and in-node were the most likely to exhibit propagation (Fig. 3C).

To disentangle the effect of FR-Delta coupling from FR propagation we examined the preferred phase angle distributions of propagating and non-propagating FR with respect to delta. Overall, in the SOZ and NSOZ out-node and in-node, propagating FR, across pooled edges, showed a preferred phase angle near the peak of delta (Fig. 3D, Table S6). In the out-node, the preferred phase angle of the FR-Delta coupling was during the ascending portion of the wave slightly before the peak, as compared with the in-node where the preferred phase angle was nearer to the peak. For FR recorded from the SOZ in limbic structures, propagated FR occurred earlier before the peak and precessed more of the delta wave at the in-node as compared with the non-propagating distributions (Bayesian mixed-effect regression model for circular data, bpnreg[18], Bayes Factor (BF) 2 of 2 for interaction of propagation status and node status compared to node status for predicting FR-Delta phase angle, Fig. 3D1-2, Table S6). In the frontal lobe and the parietal lobe SOZ, node status predicted the FR-Delta preferred phase angle more than propagation status, or the nodal status and propagation interaction (bpnreg, BF 1.98/2 frontal, BF 2/2 parietal node status compared to propagation status, Fig. 3C1-2, Table S6). Pooling of individual edges may have contributed to regions where the phase angle distribution showed weak or no FR-Delta phase locking. In our bpnreg models, edge number was used as the random effect to control for such variability.

In the NSOZ, limbic FR-Delta angle distributions were not phase locked in the non-propagating FR (Figure S9, Table S7). However, in other regions, phase locking was observed for non-propagating FR in the in-node (Figure S9, Table S7). In the case of propagating FR in the NSOZ, FR-Delta phase locking was observed at both the in-node and out-node (Fig. 3C4, Table S7). Despite these observations at the pooled group level, our model indicated in the NSOZ, the interaction between node status and propagation status predicted FR-Delta phase angle distributions as well as node status and propagation status alone (bpnreg, Table S7).

Since recording the iEEG in either a referential or bipolar montage can influence both the properties of FR and FR-Delta coupling, we examined the effects of montage in our GLMMs (Table S2-S4) and our bpnreg models (Table S6, S7). Montage accounted for a small portion of the outcome for the GLMMs (Table S2-S4). In the bpnreg models, montage accounted for almost none of the phase angle prediction in the limbic SOZ (BF 0.04/2, Table S6), but in the temporal SOZ was a significant confound (BF 2/2, Table S6).

Most of the FR in the analysis were recorded from limbic SOZ regions (Fig. 3C). Limited sample size and sampling bias could have influenced our observations in the other neuroanatomical locations and the NSOZ. In the limbic SOZ, FR-delta coupling does appear to drive FR generation, and be an important

factor promoting propagation, independent of whether the FR is propagated. However, propagation appears to be a distinct mechanism because it is associated with a larger delta wave phase precession to the peak.

Spikes and sharp waves follow propagated fast ripples at the out node

Having established that, in patients with epilepsy, delta oscillations in the limbic SOZ putatively drive the generation of FR, and that FR propagation is an event associated with, but distinct from, this coupling, we next sought to quantify our visual observations (Fig. 1A,S3A,S7A) and determine if FR propagation is associated with the generation of epileptiform spikes and sharp-waves in the intracranial EEG. To quantify changes in the iEEG and epileptiform activity following propagating FR, we accounted for the fact that power spectral densities (PSD) and time-frequency spectrograms of epileptiform spikes demonstrate a broad band increase in power associated with the sharp transients of an epileptiform spike's positive and negative going components[19]. The broad band power increases have also been associated with increased neuronal activation[20–22] and measured using the aperiodic offset of the fit power spectral density[23].

To assess if FR propagation is associated with the initiation of epileptiform spikes and sharp waves, we separated the propagated from non-propagated FR and created one second iEEG trials with the FR onset time aligned at 250 ms. Visual inspection confirmed our automated detection system methodology assuring that in each trial, the FR onset occurred before the initial positive or negative phase of the spike[15] (Fig. 1A, S3A,S7A). From these trials we measured the FR-related modulation of the post-FR iEEG signal. As part of this analysis, the occurrence of the FR in the out-node was also used as a trigger for generating one second iEEG trials in the in-node to measure cross-modulation and confirm propagation. Additionally, for each set of propagated, or non-propagated, FR-triggered iEEG trials from the in-node or out-node we calculated the average fit power spectral density[23]. We found that 8 of the 29 SOZ:SOZ edges exhibited propagating FR triggered epileptiform spikes in the out- and sometimes also in-node, but in these cases, we did not observe spikes associated with non-propagating FR (Fig. 4A,B). In another 12 of the 29 SOZ:SOZ edges, a FR triggered spike or sharp-wave was seen following both propagated and non-propagated FR at the out- and in-node, but the modulation of the spike was larger following the propagated fast ripples (Fig. 4C,D,S10,S11). In one patient, who had longer propagation delays (Fig. 1C1) and longer duration FR (Figure S3B), FR propagation was associated with the onset of a sharply contoured delta wave (Figure S12). To quantify these differences, we examined the aperiodic and periodic parameters of the PSD fits and compared propagating FRs with non-propagating FRs in the out- and in-node. We found that in the out-node, but not the in-node, the FR-iEEG trials associated with propagating FRs had a larger aperiodic offset and peak frequency (paired t-tests, d.f.=28, Benjamani-Hochberg adj-p = 0.03, 0.02, Fig. 4E1, E3, Table S8). As a control, we also performed an identical comparison of the FR-iEEG trials one second before the aligned FR events and found no significant differences (adj-p > 0.05, Fig. 4E, Table S8). These quantitative results support that propagating FR events in the SOZ precede epileptiform spikes and sharp-waves.

Since the propagating and non-propagating FR exhibited distinct properties (Fig. 2, Table S2-S4), it was required to determine whether the FR propagation status or the FR properties were more predictive of an after-going epileptiform spike. We used a GLMM to predict the aperiodic offset of individual iEEG trials in the out-node, for events in SOZ:SOZ edges, using the accompanying FR's propagation status, power, frequency, and duration. We found that the propagation status of the FR predicted the aperiodic offset magnitude (GLMM, $p < 1e\text{-}26$, Table S9), but not FR power, frequency, duration, or the interaction of FR power with propagation status (GLMM, $p > 0.05$, Table S9).

When this cross-modulation and PSD fitting approach was applied to NSOZ:SOZ, SOZ:NSOZ, and NSOZ:NSOZ edges heterogenous results were found. In one NSOZ:SOZ edge propagating FR resulted in a more strongly modulated spike in the in-node but not the out-node (Figure S13), but this was not the case for other edges bordering the two territories. For the NSOZ:NSOZ edges, most commonly no epileptiform spike or sharp wave followed FR propagation (Fig. 5A,B), although in one edge a sharp wave was seen in the out-node (Figure S14). Another patient with NSOZ:NSOZ edges exhibited extremely long FR (Figure S4) but no strong cross-modulation (Figure S15). Across all the NSOZ:SOZ, SOZ:NSOZ, and NSOZ:NSOZ edges, in the out- or in-node, the aperiodic and periodic parameter differences of the PSD fits between propagating and non-propagating events did not reach significance (adj-$p > 0.05$, Fig. 5C, Table S10) indicating that FR propagation outside of the SOZ appears to be by distinct mechanisms that, in contrast to the SOZ:SOZ edges, do not usually precede epileptiform spikes.

Discussion

We demonstrate that, in accord with past observations[13], unidirectional FR propagation, at relatively slow velocities, occurs in patients with medically refractory epilepsy. By differentiating the propagating and non-propagating FR, we found that the spectral content and power of propagating FR at the origin was higher lending support that putative propagating FR events were associated with network level phenomena distinct from that of a common external or coincident internal driver between the FR out-node and in-node. FR generation was also strongly phase coupled to sleep delta oscillations both at the origin and destination of the FR propagation, but coupled events occurred relatively earlier before the peak of the delta wave. This indicates that while FR-delta coupling coordinates and drives FR generation across wide-spread brain regions, FR propagation is a unique mechanism. Finally, we found that in the SOZ propagating FR were associated with subsequent time locked epileptiform spikes and quantifiable changes in the power spectrum associated with increased neuronal activation[20–22]. These results offer mechanistic insights into the epileptic network[2] through the demonstration of a state dependent change in network excitability generated by propagating FR (Fig. 6).

Mechanisms of FR generation and propagation

FR may be generated by action or synaptic currents[8]. Due to channel kinetics, it is debatable if synaptic currents could reliably generate FR with a spectral content > 350 Hz. However, chloride homeostasis

disruption in pathologic neurons is known to contribute to epileptic discharges[24,25] and FR generation[26]. Modeling studies have shown that FR and inter-ictal spikes both involve depolarizing $GABA_A$ reversal potentials, but during IEDs relatively more pyramidal neurons fire action potentials, with a higher degree synchrony, than during a FR[27]. The kinetics of GABAergic fast inhibitory potentials are sufficiently rapid to account for > 350 Hz FR with a 1 ms rise time and 11 ms decay time[28]. Synchronized, but out of phase[29], firing of inhibitory interneurons could also further facilitate > 350 Hz FR generation. The presence of the > 350 Hz FR in our macroelectrode recordings supports that the events are generated by synaptic and not action currents[30], since action currents would be more likely to exhibit phase cancellation due to the large electrode contact surface area. In contrast, in microelectrode recordings action currents do contribute to the FR[8,9].

With respect to the mechanism of FR propagation, in the healthy hippocampus, SPW-R power is correlated with the degree of SPW-R propagation across the septo-temporal axis[31]. Also, higher power SPW-R propagate from dorsal CA1 to the granular retrosplenial cortex through the subiculum via the transiently increased drive of both excitatory and inhibitory neurons and their synaptic interactions[32,33], as opposed to via electrical transmission[34]. Potentially FR propagation could occur under similar synaptic mechanisms involving GABA-mediated depolarizing potentials when a supra-threshold number of neurons are recruited.

Implications of FR-Delta Coupling

The strong coupling of FR to the peak of the delta wave, across widespread brain regions[16,17], and in our study primarily in limbic epileptogenic regions, is in accord with FR generation by GABA-mediated depolarizing potentials and would otherwise be paradoxical. A significant portion of the delta waves are part of the slow wave that modulates excitability during non-REM sleep[35]. Thus, the peak of the delta wave corresponds to the DOWN state and until recently the DOWN state was associated with a paucity of neuronal activity including in intracranial human data[36]. Recent evidence suggests that at the positive peak of these slow/delta oscillation inhibitory ID2/Nkx2.1 barrage firing[37] neurogliaform cells[38], and select populations of pyramidal neurons[39] are activated. If PIN clusters, endowed with depolarizing $GABA_A$ reversal potentials[25,26,40], receive synaptic drive from these DOWN state active populations, it could potentially result in a FR while the same synaptic drive to surrounding non-pathologic neurons would be hyperpolarizing and contribute to the extracellular positive peak of the slow/delta oscillation and surround inhibition[37].

Additionally, propagating FR occurred earlier during the UP-DOWN transition and have greater power than non-propagating FR. This suggests that the slope of the synaptic depolarizing drive on to the PIN cluster neurons during the UP-DOWN transition is steeper for the propagating FR events. At nodes in which FR propagation did not occur, coupling with slow/delta oscillations was weak or absent, indicating that depolarizing inhibitory potentials of the slow wave may not have strongly contributed to FR generation there. Also, the differences between the timing, with respect to slow/delta peak, of the non-propagating

FR in the out-node and in-node could also relate to the slope of the synaptic depolarizing drive at the two locations. In line with this hypothesis is that the FR exhibited a smaller power at the in-node.

Propagating FR, epileptic spikes, and inhibitory restraint

We propose that at the time and location of the FR, an inhibitory restraint mechanism[6,7], mediated by inhibitory synaptic potentials in neurons surrounding PIN clusters, may normally prevent FR propagation. Notably, in murine models, bicuculline application has been shown to expand the volume of the tissue generating FR, and FR have previously been proposed to overcome an inhibitory restraint to trigger seizure activity[8]. A similar restraint mechanism may normally prevent FR from promoting epileptiform spikes caused by the hyper-synchronization of pyramidal neurons. We found that only the higher-power FR, with stronger recruitment, propagated and were more likely to precede epileptiform spikes suggesting that for those events synaptic excitation overcame the surrounding inhibition (Fig. 6).

The unidirectional pattern of the FR propagation suggests that FR propagation may involve successively recruiting neighboring PIN clusters, and thus the propagating FR is restrained to epileptogenic tissue[10]. In contrast, the resulting epileptiform spikes may propagate by other synaptic and ephaptic mechanisms[41] across healthy tissue and can thus be found outside epileptogenic regions[42].

In the NSOZ, propagating FR do not often precede IEDs but could be clinically meaningful because failure of epilepsy surgery can result from leaving NSOZ FR-generating regions intact[10]. An important consideration is that patients who do not respond to surgery have widespread and highly active asynchronous FR generating sites, either inside or outside the SOZ[12]. A highly asynchronous FR network may be a result of a breakdown in inhibitory restraint that affects a multitude of nodes and edges in the network. In such a network, FR propagation may not correlate with epileptiform spikes or seizures because of the putative widespread propagation of FR and loss of surround inhibition. Further efforts are required to relate FR propagation in the NSOZ to asynchronous FR networks to better understand seizure genesis there.

Conclusion

In summary, we have found that FR propagate in the SOZ and between the SOZ and NSOZ by distinct mechanisms. In the SOZ, FR propagate slowly (~ 1.54 mm/ms) from the out-node, contain higher spectral frequency and power than non-propagating FR. FR couple to the peak of slow/delta oscillations during non-REM sleep and strong coupling is a prerequisite for FR propagation. The preferred phase angle of coupling differs between the out-node and in-node and propagating FR occur earlier before the slow/delta peak in the out-node. The propagating FR events in the SOZ are more likely to be time-locked to after-going epileptiform spikes. These results support an inhibitory restraint mechanism preventing amplification and propagation of epileptic activity from definable pathologic sites in a network, since propagating FR with hyperexcitability were more strongly associated with after-going epileptiform spikes[6,7]. Future experiments utilizing animal models of focal seizures using *in vivo* patch clamp, calcium

and chloride imaging, and optogenetics are required to test the mechanistic implications of our iEEG recordings in patients.

Methods

All data were acquired with approval from the local institutional review board (IRB) at each clinical institution: TJU by the IRB of Thomas Jefferson University; UCLA by the IRB University of California Los Angeles. Informed consent was given at each clinical center. The acquisition of data for research purposes was completed with no impact on the clinical objectives of the patient stay. Digitized

data were stored in an IRB-approved database compliant with Health Insurance Portability and Accountability Act regulations.

Dataset collection

This retrospective mechanistic study of epileptogenicity biomarkers used consecutive recordings selected from 19 patients who underwent intracranial monitoring with depth electrodes between 2014–2018 at University of California Los Angeles (UCLA) and from 27 patients at Thomas Jefferson University (TJU) in 2016–2018 for the purpose of localization of the seizure onset zone. Patients had pre-surgical magnetic resonance imaging (MRI) for MRI-guided stereotactic electrode implantation, as well as a post-implant CT scan to localize the electrodes. The inclusion criteria were at least one night of intracranial recording at a 2000 Hz sampling rate uninterrupted by seizures and at least 4 h of interictal non-REM iEEG recordings. One to two days after implantation, for each patient a 10 to 60 minutes iEEG recording from all the depth electrodes that contained large amplitude, slow and delta-frequency waves (i.e., non-REM sleep) was selected for analysis. Only iEEG that was free of low levels of muscle contamination and other artifacts was selected. Among all patients enrolled in the research study, recordings that met the inclusion criteria were available for approximately 60% of the UCLA patients, and 80% of the TJU patients. At UCLA research recordings were not always performed. No other patients were excluded on any other basis. The attending neurologist determined the seizure onset zone from visual inspection of video-EEG during the patient's habitual seizures. The seizure onset zone was aggregated across all these seizures during the entire iEEG evaluation for each patient and did not include areas of early propagation. The non-SOZ included all remaining contacts and was often separated from the SOZ by sub-centimeter distances.

T1- and T2-weighted MRIs were obtained for each patient, prior to electrode implantation. FreeSurfer (http://surfer.nmr.mgh.harvard.edu/) was used on the T1-weighted MRI to construct individual subject brain surfaces and cortical parcellations according to the Desikan–Killiany atlas[43]. With the assistance of a neuroradiologist the Advanced Neuroimaging Tools [44] was used to coregister the post-implantation CT with the pre-implantation MRI, and the position of each electrode contact was localized to the Desikan-Killiany atlas. Then an in-house pipeline (https://github.com/pennmem/neurorad_pipeline) was used to transform the position of each electrode contact from individual subject space to an averaged

FreeSurfer space with normalized Montreal Neurological Institute (MNI) coordinates (defined by the fsaverage brain).

For each patient, clinical iEEG (0.1–600 Hz; 2000 samples per second) was recorded from 8–16 depth electrodes, each with 7 to 15 contacts, using a Nihon-Kohden 256-channel JE-120 long-term monitoring system (Nihon-Kohden America, Foothill Ranch, CA, U.S.A.). A larger number of electrodes with more contacts were implanted at TJU. The reference signal used for the recordings performed at UCLA was a scalp electrode position at Fz in the International 10–20 System. The reference signal used for the TJU recordings was an electrode in the white matter.

HFO detection and characterization

HFOs and sharp-spikes were detected in the non-REM sleep iEEG using previously published methods[12,45,46] implemented in Matlab (Mathworks, Natick, MA, USA). In brief, the HFO detector reduced muscle and electrode artifacts in the iEEG recordings using an independent component analysis (ICA)-based algorithm[46]. After applying this ICA-based method, ripples and fast ripples were detected in the referential and bipolar montage iEEG recordings per contact by utilizing a Hilbert detector, in which a 1,000th order symmetric finite impulse response (FIR) band-pass filter in the 250–600 Hz band for fast ripples was applied, and (ii) a Hilbert transform was applied to calculate the instantaneous amplitude of this time series according to the analytic signal z(t) in Eq. 1.

$$z(t) = a(t)e^{i\theta(t)}$$

where a(t) is the instantaneous amplitude and θ(t) is the instantaneous phase of z(t). Following the Hilbert transform, the instantaneous HFO amplitude function [a(t)] was smoothed using moving window averaging, the smoothed instantaneous HFO amplitude function was normalized using the mean and standard deviation of the time series, and a statistical threshold defined by the skewness of the normalized band pass filtered time series was used to detect the onset and offset of discrete/potential events.

HFO-like events can arise due to Gibb's phenomenon, i.e., high-pass filtering sharp transients, including epileptiform spikes[19]. To distinguish authentic HFOs from authentic HFOs on EEG spikes or spurious HFO due to filter ringing, we used an algorithm that performed topographic analysis of time-frequency plots for each HFO and defined open- and closed-loop contour groups (Fig. 1B)[45]. The algorithm also measured the power, spectral content, duration, onset time, and offset time of each HFO and categorized the HFO as an HFO on oscillation, HFO on spike, or sharp-spike (*i.e.* false HFO)[19]. HFOs that did not coincide with spikes were defined as closed-loop contour groups with an onset and offset that did not overlap with the onset or offset of open-loop contour groups. For HFOs on spikes the two groups temporally overlapped[45].

To measure FR-delta coupling an optimized Hamming-windowed FIR band-pass filter (eegfiltnew.m; EEGLAB, https://sccn.ucsd.edu/eeglab) was applied to the iEEG recordings in the delta (2–4 Hz) band.

We then calculated the instantaneous amplitude of the Hilbert transformed band-pass filtered signal (Eq. 1). The instantaneous amplitude was normalized, and we used minimum amplitude and duration criteria to identify epochs in which oscillatory delta bursts appeared. This calibration was performed blinded to the fast ripple detections and adjusted and optimized based on visual inspection of annotated unfiltered iEEG recordings. After identifying the epochs of delta bursts, FR coinciding with delta were identified using the fast ripple onset times. we transformed each fast ripple event into a phasor, as described in Eq. 2.

$$ve^{i\theta}\sum_{t}^{T}\alpha(t)\,e^{i\omega t}$$

where v is the vector strength of the phasor, theta its phase angle, and a(t) and ω(t) are the respective instantaneous fast ripple amplitude and iEEG delta phase during the fast ripple ripple across its duration [t.T][47]. A derivative of this method was used to generate our example delta band filtered iEEG example and corresponding instantaneous phase. Our open source HFO detector with these features, and others, can be downloaded from http://github.com/shenweiss. Following automatic detection of HFO and sharp-spikes, false detections of clear muscle and mechanical artifact were deleted by visual review in Micromed Brainquick (Venice, Italy). After the redactions, each HFO and spike along with its properties (spectral frequency, duration, power, coupling information, neuroanatomic contact location, and clinical metadata) were stored in a MongoDB database for further analysis.

Identifying fast ripple propagation and distinguishing propagated events

For each pair of electrode contacts generating fast ripples, within patients, we measured the mutual information (MI) of the fast ripple onset times between the two pairs[12,48]. If the mutual information was greater than zero, we used the sign test for zero median in Matlab (signtest.m) to assess unidirectional propagation. To perform this test, we subtracted the onset times of fast ripples from one contact with the onset times of fast ripples in the other contact using the meshgrid.m function. Differences exceeding ± 250 + ms were excluded[13]. Using the false discovery rate of 0.05, a p-value cutoff of 0.005 for the sign test was selected based on multiple comparison testing using the Benjamini-Hochberg false detection ratio (bh_fdr.m) for contact pairs with 120 fast ripples each. All edges showing significant propagation were visually inspected and if fast ripple propagation was not observed they were excluded. Contact pairs showing significant propagation with less than 120 fast ripples each were also tested in cross-modulation experiments (see Cross-modulation). The propagated fast ripples, in an edge showing statistically significant unidirectional propagation, were distinguished in the out contact and in contact by occurring within ± 250 ms of each other.

Generalized linear mixed effects models and linear regression

HFO frequency, power and duration values were fit with generalized linear mixed-effects models (GLMMs) in Matlab using the fitglme.m function with a fixed intercept and Laplace fit method. The edge number was at which the fast ripple was detected was the random-effects term. The fixed effect predictors included out or in status and montage status (*i.e.*, referential or bipolar) of the contact, the propagation status of the fast ripple, the mean delay of fast ripples in the propagating edge, the distance between the nodes in the edge, and the SOZ status (*i.e.* SOZ or NSOZ) of each contact in the edge. Interaction terms were also included. A GLMM was used to fit the sign test Z value of all edges with a fast ripple MI greater than zero. A fixed intercept was used. The patient number for each edge was the random effects term. The fixed effects term was the Rayleigh test Z value (see circular statistics) of FR-delta coupling in the out and in node, and the SOZ status of the nodes in the edge. Interaction terms were also included. Also, a GLMM was used to fit the fitted power spectral density aperiodic offset value with a fixed intercept and maximum pseudo-likelihood method in which the edge number was the random effect term, and the FR propagation status, FR frequency, FR duration, and FR power. Interaction terms were also included. Linear models comparing mean fast ripple number per electrode contact to the number of propagating edges, or propagation distance (derived as the Euclidian distance in mm using the MNI coordinate system) with propagation delay were performed using fitlm.m.

Circular statistics and brain renderings

The significance and strength of FR-delta coupling was measured using the Rayleigh test (circ_rtest.m) applied to the FR phasors measured at a given node. The circ_mean.m function was used to measure the mean phase angles and 95% confidence intervals of the FR phasor phase angles. A Bayesian projected normal regression model for circular data (bpnreg)[18], implemented in R, was used to fit the FR phasor angles using a random effects term of the pair number, and fixed effects predictors of the out and in status of the contact, the montage of the contact, the propagation status of the fast ripple, and the interaction of the out and in status with the propagation status. To visualize the location of nodes exhibiting statistically significant FR-delta coupling, we used brainnet viewer[49]. Propagated edges in MNI space were generated in Matlab using the quiver3.m function.

Cross-modulation

To identify and characterize the low-frequency waveforms and oscillations that modulate fast ripple amplitude and are modulated by the occurrence of fast ripples, we used a event-triggered coupling methodology[50]. Trials of unfiltered iEEG, 1 s in duration, aligned by the onset time of the fast ripple events in the out node at 250 ms were summated to derive a modulatory signal. The statistical significance of the modulatory signal was derived by computing 300 surrogates using phase shuffling and calculating the peak-to-peak amplitude of the randomized signals. The modulated signal was calculated by convolving each 1 s unfiltered iEEG trial, with a fast ripple occurring at 250 msec, with complex Morlet wavelets with a width of seven cycles, and a standard deviation of three cycles using Fieldtrip (http://www.fieldtriptoolbox.org/). The time-frequency representations for each trial were then averaged and normalized (using a z-score) to account for (1/f) spectral power. To measure cross-modulation and confirm that fast ripple propagation had taken place in the in node, fast ripple events in the out node were

used to generate 1 s trials in the in node, irrespective of whether a fast ripple had been measured at that time there, and the event-triggered methodology was applied.

Power spectral density fitting and statistics

A Welch power spectral density (psd) was applied to the 1 s fast ripple aligned trials in the out- node and corresponding 1 s trials in the in-node in Python using MNE (https://mne.tools/). Trials generated one second prior to these trials were also examined as a control. The length of the fast Fourier transform was 1000 samples, the number of overlapping points between segments was 250 samples. The periodic and aperiodic components of the PSD were fit using fitting oscillations & one over f (fooof, https://fooof-tools.github.io/fooof/)[23] which uses a Lorentzian function. We fit a peak between 1 to 6 Hz. In one experiment we derived the aperiodic and periodic parameters from the individual trials, and in another fooof fits from the individual power spectra derived from either the propagating or non-propagating events in the out node, or the corresponding events in the in node were combined using the combine_fooofs function to derive the average aperiodic and periodic parameters. These parameters were compared between propagating and non-propagating events using a paired t-test (ttest.m) and adjusted for multiple comparisons within each group using the Benjamini-Hochberg method (bh_fdr.m) with a false discovery rate of 0.05. A psd was also applied to the full recording duration 20–60 minutes using a Welch psd with a 20 second window.

Data availability

Due to their large size, the complete collection of unprocessed iEEG data files is available upon reasonable request from the authors. The unprocessed iEEG data used for figure generation in this paper is available at https://www.zenodo.org/record/6529724#.Ynkv4YfML9Y and https://zenodo.org/record/6532325#.YnlLF4fML9Y. The processed HFO and electrode contact MongoDB JSON files collected from all the recruited patients can be downloaded from https://zenodo.org/record/6451900#.YmgQie3ML9Y and is used by our code to generate figures and for statistical purposes.

Code availability

All the code for processing the iEEG data files, performing statistics, and generating figures are available as open source from https://github.com/shenweiss/publishedcode.

References

1. *Epilepsy, a comprehensive textbook. 2nd ed.* (Wolters Kluwer/Lippincott Williams & Wilkins, 2008).
2. Davis, K. A., Jirsa, V. K. & Schevon, C. A. Wheels Within Wheels: Theory and Practice of Epileptic Networks. Epilepsy Curr 153575972110156 (2021) doi:10.1177/15357597211015663.
3. Hatton, S. N. *et al.* White matter abnormalities across different epilepsy syndromes in adults: an ENIGMA-Epilepsy study. Brain 143, 2454–2473 (2020).

4. Englot, D. J., Konrad, P. E. & Morgan, V. L. Regional and global connectivity disturbances in focal epilepsy, related neurocognitive sequelae, and potential mechanistic underpinnings. Epilepsia 57, 1546–1557 (2016).
5. Sinha, N. *et al.* Predicting neurosurgical outcomes in focal epilepsy patients using computational modelling. Brain 140, 319–332 (2017).
6. Trevelyan, A. J., Sussillo, D., Watson, B. O. & Yuste, R. Modular Propagation of Epileptiform Activity: Evidence for an Inhibitory Veto in Neocortex. J Neurosci 26, 12447–12455 (2006).
7. Schevon, C. A. *et al.* Evidence of an inhibitory restraint of seizure activity in humans. Nat Commun 3, 1060 (2012).
8. Bragin, A., Mody, I., Wilson, C. L. & Engel, J. Local Generation of Fast Ripples in Epileptic Brain. J Neurosci 22, 2012–2021 (2002).
9. Bragin, A., Benassi, S. K., Kheiri, F. & Engel, J. Further evidence that pathologic high-frequency oscillations are bursts of population spikes derived from recordings of identified cells in dentate gyrus. Epilepsia 52, 45–52 (2011).
10. Nevalainen, P. *et al.* Association of fast ripples on intracranial EEG and outcomes after epilepsy surgery. Neurology 95, e2235–e2245 (2020).
11. Weiss, S. A. *et al.* Ictal onset patterns of local field potentials, high frequency oscillations, and unit activity in human mesial temporal lobe epilepsy. Epilepsia 57, 111–121 (2016).
12. Weiss, S. A. *et al.* Graph theoretical measures of fast ripples support the epileptic network hypothesis. Brain Commun (2022) doi:10.1093/braincomms/fcac101.
13. Otárula, K. A. G., Ellenrieder, N. von, Cuello-Oderiz, C., Dubeau, F. & Gotman, J. High-Frequency Oscillation Networks and Surgical Outcome in Adult Focal Epilepsy. Ann Neurol 85, 485–494 (2019).
14. Khambhati, A. N., Sizemore, A. E., Betzel, R. F. & Bassett, D. S. Modeling and interpreting mesoscale network dynamics. Neuroimage 180, 337–349 (2018).
15. Guth, T. A. *et al.* Interictal spikes with and without high-frequency oscillation have different single-neuron correlates. Brain (2021) doi:10.1093/brain/awab288.
16. Sheybani, L. *et al.* Electrophysiological Evidence for the Development of a Self-Sustained Large-Scale Epileptic Network in the Kainate Mouse Model of Temporal Lobe Epilepsy. J Neurosci 38, 3776–3791 (2018).
17. Sheybani, L., Mierlo, P. van, Birot, G., Michel, C. M. & Quairiaux, C. Large-scale 3–5 Hz oscillation constrains the expression of neocortical fast-ripples in a mouse model of mesial temporal lobe epilepsy. Eneuro 6, ENEURO.0494-18.2019 (2019).
18. Cremers, J. & Klugkist, I. One Direction? A Tutorial for Circular Data Analysis Using R With Examples in Cognitive Psychology. Front Psychol 9, 2040 (2018).
19. Bénar, C. G., Chauvière, L., Bartolomei, F. & Wendling, F. Pitfalls of high-pass filtering for detecting epileptic oscillations: A technical note on “false” ripples. Clin Neurophysiol 121, 301–310 (2010).

20. Manning, J. R., Jacobs, J., Fried, I. & Kahana, M. J. Broadband shifts in local field potential power spectra are correlated with single-neuron spiking in humans. J Neurosci Official J Soc Neurosci 29, 13613–20 (2009).
21. Miller, K. J. *et al.* Human Motor Cortical Activity Is Selectively Phase-Entrained on Underlying Rhythms. Plos Comput Biol 8, e1002655 (2012).
22. Winawer, J. *et al.* Asynchronous Broadband Signals Are the Principal Source of the BOLD Response in Human Visual Cortex. Curr Biol 23, 1145–1153 (2013).
23. Donoghue, T. *et al.* Parameterizing neural power spectra into periodic and aperiodic components. Nat Neurosci 23, 1655–1665 (2020).
24. Cohen, I., Navarro, V., Clemenceau, S., Baulac, M. & Miles, R. On the Origin of Interictal Activity in Human Temporal Lobe Epilepsy in Vitro. Science 298, 1418–1421 (2002).
25. Huberfeld, G. *et al.* Perturbed Chloride Homeostasis and GABAergic Signaling in Human Temporal Lobe Epilepsy. J Neurosci 27, 9866–9873 (2007).
26. Alfonsa, H. *et al.* The contribution of raised intraneuronal chloride to epileptic network activity. J Neurosci Official J Soc Neurosci 35, 7715–26 (2015).
27. Demont-Guignard, S. *et al.* Distinct hyperexcitability mechanisms underlie fast ripples and epileptic spikes. Ann Neurol 71, 342–352 (2012).
28. Strüber, M., Jonas, P. & Bartos, M. Strength and duration of perisomatic GABAergic inhibition depend on distance between synaptically connected cells. P Natl Acad Sci Usa 112, 1220–5 (2015).
29. Foffani, G., Uzcategui, Y. G., Gal, B. & Prida, L. M. de la. Reduced Spike-Timing Reliability Correlates with the Emergence of Fast Ripples in the Rat Epileptic Hippocampus. Neuron 55, 930–941 (2007).
30. Shamas, M. *et al.* On the origin of epileptic High Frequency Oscillations observed on clinical electrodes. Clin Neurophysiol 129, 829–841 (2018).
31. Patel, J., Schomburg, E. W., Berényi, A., Fujisawa, S. & Buzsáki, G. Local Generation and Propagation of Ripples along the Septotemporal Axis of the Hippocampus. J Neurosci 33, 17029–17041 (2013).
32. Stark, E. *et al.* Pyramidal Cell-Interneuron Interactions Underlie Hippocampal Ripple Oscillations. Neuron 83, 467–480 (2014).
33. Nitzan, N. *et al.* Propagation of hippocampal ripples to the neocortex by way of a subiculum-retrosplenial pathway. Nat Commun 11, 1947 (2020).
34. Simon, A. *et al.* Gap junction networks can generate both ripple-like and fast ripple-like oscillations. Eur J Neurosci 39, 46–60 (2014).
35. Sirota, A., Csicsvari, J., Buhl, D. & Buzsáki, G. Communication between neocortex and hippocampus during sleep in rodents. Proc National Acad Sci 100, 2065–2069 (2003).
36. Nir, Y. *et al.* Regional Slow Waves and Spindles in Human Sleep. Neuron 70, 153–169 (2011).
37. Chittajallu, R. *et al.* Activity-dependent tuning of intrinsic excitability in mouse and human neurogliaform cells. Elife 9, e57571 (2020).

38. Valero, M. *et al.* Sleep down state-active ID2/Nkx2.1 interneurons in the neocortex. Nat Neurosci 24, 401–411 (2021).
39. Todorova, R. & Zugaro, M. Isolated cortical computations during delta waves support memory consolidation. Science 366, 377–381 (2019).
40. Pallud, J. *et al.* Cortical GABAergic excitation contributes to epileptic activities around human glioma. Sci Transl Med 6, 244ra89-244ra89 (2014).
41. Shivacharan, R. S. *et al.* Neural recruitment by ephaptic coupling in epilepsy. Epilepsia 62, 1505–1517 (2021).
42. Azeem, A. *et al.* Interictal spike networks predict surgical outcome in patients with drug-resistant focal epilepsy. Ann Clin Transl Neur 8, 1212–1223 (2021).
43. Desikan, R. S. *et al.* An automated labeling system for subdividing the human cerebral cortex on MRI scans into gyral based regions of interest. Neuroimage 31, 968–980 (2006).
44. Avants, B. B., Epstein, C. L., Grossman, M. & Gee, J. C. Symmetric diffeomorphic image registration with cross-correlation: Evaluating automated labeling of elderly and neurodegenerative brain. Med Image Anal 12, 26–41 (2008).
45. Waldman, Z. J. *et al.* A method for the topographical identification and quantification of high frequency oscillations in intracranial electroencephalography recordings. Clin Neurophysiol 129, 308–318 (2018).
46. Shimamoto, S. *et al.* Utilization of independent component analysis for accurate pathological ripple detection in intracranial EEG recordings recorded extra- and intra-operatively. Clin Neurophysiol 129, 296–307 (2018).
47. Song, I. *et al.* Bimodal coupling of ripples and slower oscillations during sleep in patients with focal epilepsy. Epilepsia 58, 1972–1984 (2017).
48. Gribkova, E. D., Ibrahim, B. A. & Llano, D. A. A novel mutual information estimator to measure spike train correlations in a model thalamocortical network. J Neurophysiol 120, 2730–2744 (2018).
49. Xia, M., Wang, J. & He, Y. BrainNet Viewer: A Network Visualization Tool for Human Brain Connectomics. Plos One 8, e68910 (2013).
50. Dvorak, D. & Fenton, A. A. Toward a proper estimation of phase–amplitude coupling in neural oscillations. J Neurosci Meth 225, 42–56 (2014).

Figures

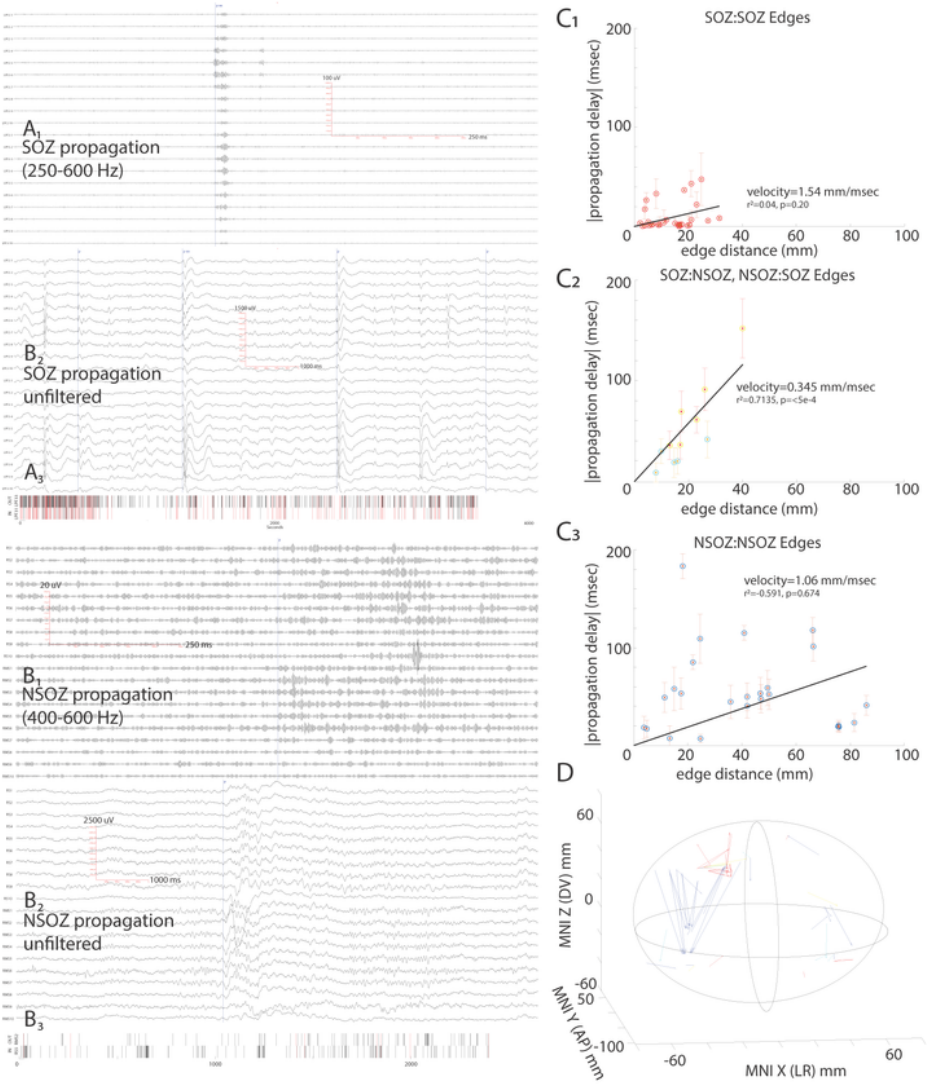

Figure 1

Fast ripples (FR) propagate in the seizure onset zone (SOZ) and non-SOZ. (A1) Example of FR propagation (vertical line labelled “p ex”) in the SOZ within the left cingulate gyrus of patient 4145 after band-pass filtering 250-600 Hz. FR propagate from the out-node (LPF3-3) to the in-node (LPF3-1), as defined by the sign test, and between other nodes not examined here. (A2) Corresponding unfiltered iEEG of same FR in A1 and other (vertical lines, “p”) propagation events, similar to A1, between these nodes.

(A3) Raster plot of FR onset times for the two nodes with statistically significant propagation (Sign test, p<1e-10). FR propagated with a mean delay of 1.6 msec across a distance of 6.4 mm. The propagating FRs (|delay|<250 msec) are denoted by red ticks. (B1) Example of FR propagation in the non-SOZ from the right paracentral lobule to the right parietal supramarginal gyrus of patient IO018 after band-pass filtering 400-600 Hz to demonstrate higher frequency FR. FR propagate from the in-node RMS2 to the out-node RS5. (B2) Corresponding unfiltered iEEG of this propagation event. (B3) Raster plot of FR for the two nodes (Sign test, p<5e-3), the mean delay was 109.1 msec across a distance of 24.5 mm. (C) Summary plot of the FR propagation velocity of edges (i.e. out-node to in-node) demonstrating significant propagation (p<5e-3) in the SOZ:SOZ (C1,red), SOZ:NSOZ (C2,yellow), NSOZ:SOZ (C2, cyan), and NSOZ:NSOZ (C3, blue). (D) Summary vector plot, in MNI coordinates, of the individual edges, color coded as in (C), demonstrating significant FR propagation across all patients, arrows point from the out-node to the in node. Circles represent borders of the cerebrum. Abbreviations (AP: anterior [+] to posterior [-], DV: dorsal [+] to ventral [-], LR: left [+] to right [-], MNI: Montreal Neurological Institute, mm: millimeters.

Figure 2

Fast ripple (FR) frequency and power differs between propagating and non-propagating FR in the out- and in-node and is dependent on the mean delay of propagation. (A) Mean FR frequency and standard error for out-node non-propagating FR (blue), out-node propagating FR (yellow), in-node non-propagating FR (red), and in-node propagating FR (cyan) for each electrode contact edge in the seizure onset zone (SOZ, A1), edges that include contacts between the SOZ and non-SOZ (NSOZ:SOZ, A2), and edges in the non-SOZ (NSOZ, A3). The four-way interaction of whether the node was out- or in- relative to the propagation (node status), if the FR was propagating (propagation status), the mean delay of propagation, and whether the contact detecting the FR was in the SOZ (SOZ status) was significant (GLMM, p<1e-4) for predicting FR frequency. In the SOZ, in most edges with a shorter propagation delay for the propagating FR, the FRs that were non-propagating and recorded from the out-node had the lowest FR frequencies (A1). (B) Box plots of the FR power for the four event types in the SOZ (B1), NSOZ:SOZ (B2), NSOZ (B3) edges. The three-way interaction of the node status, propagation status, and SOZ status was significant (GLMM, p<1e-4) for predicting FR power. SOZ and NSOZ:SOZ pairs exhibited a decrease in power of the in-node FR events, also the mean power of propagating FR events in the out node was greater than non-propagating events in the out node (B1, B2). (C) In the out-node, propagating FR with longer delays had larger power (GLMM, p<.0001). Abbreviations, GLMM:generalized linear mixed effects model, AU:arbitrary units, out p-:out-node no propagation, in p-: in-node no propagation, out p+: out-node propagation, in p+: in-node propagation.

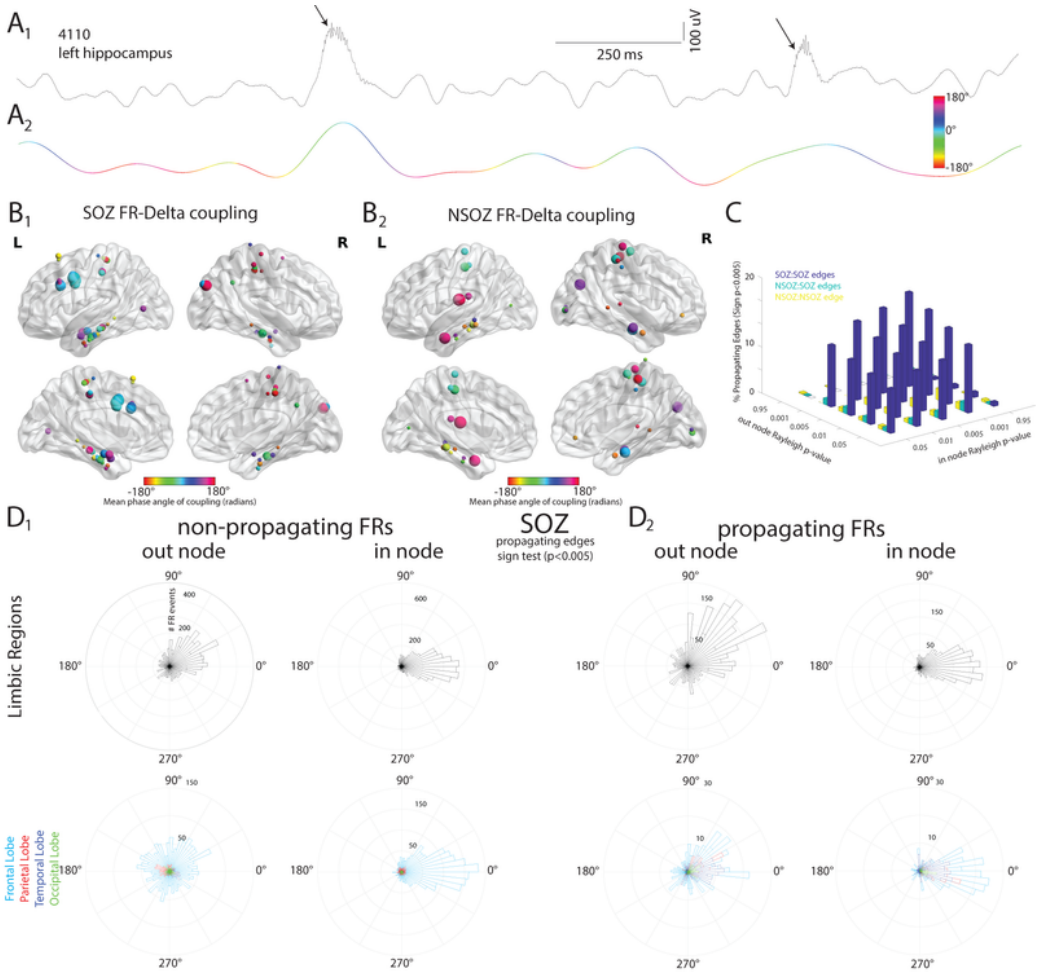

Figure 3

Fast ripple (FR) are coupled to delta oscillations and this coupling increases the probability of FR propagation between edges by a distinct mechanism. (A1) Example of FR-delta coupling in the unfiltered iEEG recorded from the SOZ. Arrows point to individual FR. (A2) Trace shown in A1 after filtering in the delta (2-4 Hz) band with instantaneous phase color coded. (B) Among the 46 patients, illustration of the aggregated nodes with statistically significant FR-delta phase coupling (Rayleigh test, p<0.001) in the

SOZ (A1) and NSOZ (A2). The size of the node indicates the Rayleigh Z value, a measure of the strength of coupling. The color of the node is the mean phase angle of coupling. (C) Three-dimensional bar plot illustrating the percentage of edges with FR mutual information > 0 and significant propagation (Sign Test, $p<0.005$) as a function of the out-node and in-node FR-delta phase coupling strength. Strength was measured as the Rayleigh test p-value for edges in the SOZ (blue), between NSOZ and SOZ or SOZ and NSOZ (green), and NSOZ (yellow). An increased sign test Z value (i.e. propagation measure) was positively correlated with higher out- and in-node FR-delta coupling strength (Rayleigh Z) in the SOZ (GLMM, $p<1e-9$). (D) Polar histograms quantifying pooled FR occurrence in relation to the phase of the delta wave. Note FR were measured only from edges with statistically significant propagation ($p<0.005$), and FR independent of a delta wave were excluded. FR-delta phase angle distributions were compared in the out- and in-node in limbic regions (black), frontal lobe (light blue), parietal lobe (red), temporal lobe (dark blue), and occipital lobe (green) for non-propagating events (D1) and propagating events (D2) in the SOZ. In limbic regions, the FR-delta coupling angle was best predicted by the interaction of whether the FR was recorded from the out- or in-node, and whether the FR event was propagated. (Bayesian mixed-effect regression model for circular data, relative Bayes Factor 2 of 2). In the frontal and parietal SOZ, the FR-delta coupling angle was best predicted by out- or in-node status than by the propagation status or the interaction (relative Bayes Factor ~2 of 2).

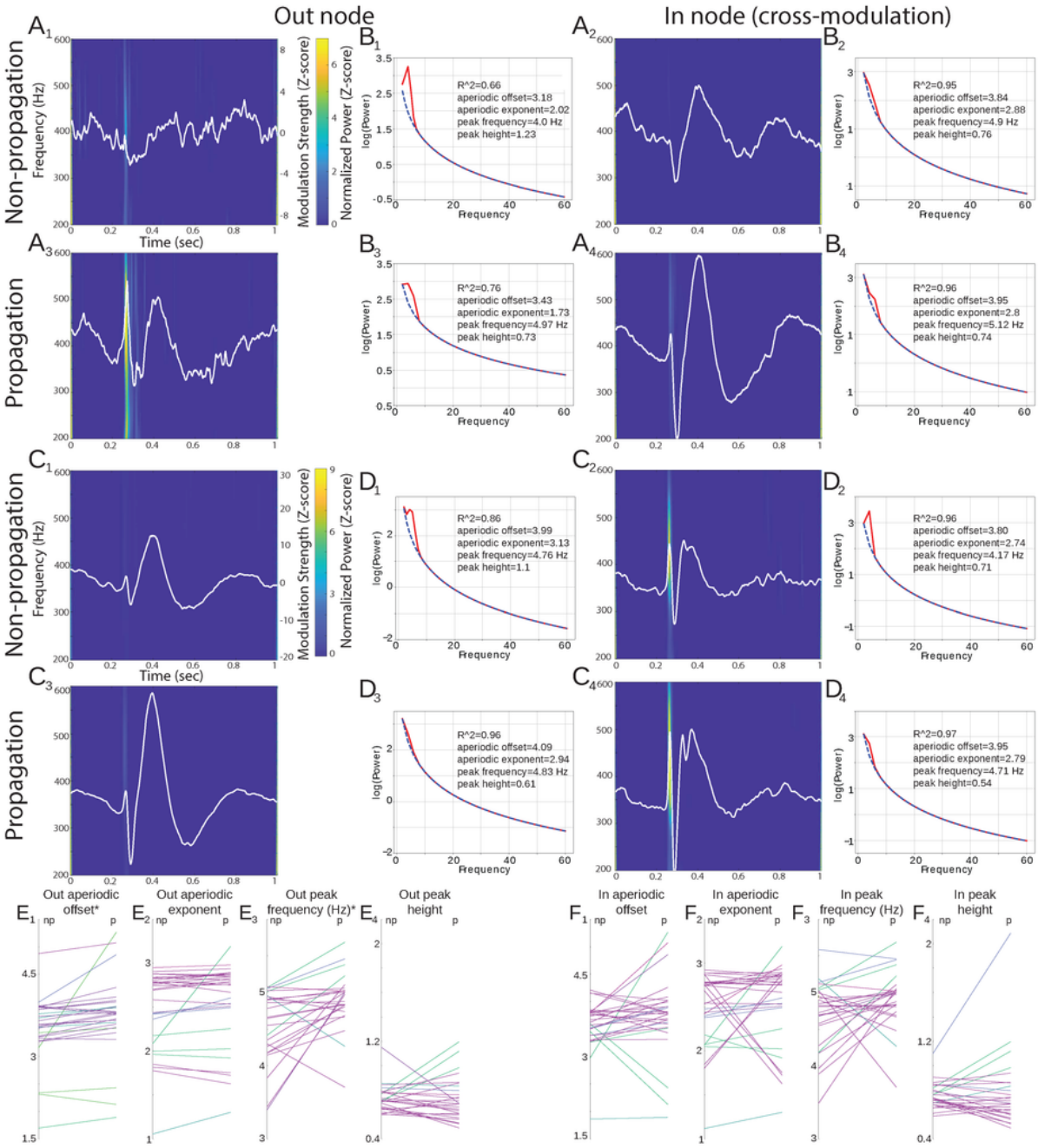

Figure 4

Fast ripple (FR) propagation and modulation to delta in the seizure onset zone (SOZ) precede epileptiform spikes in the intracranial EEG (iEEG) at the out node. (A) Example FR triggered average of iEEG signals (white traces). The peak-to-peak amplitude corresponds to the strength of modulation with FR events that are temporally aligned, with onset at 250 ms, and modulated as shown by the normalized averaged time-frequency representation. To demonstrate cross-modulation, the in-node averaged iEEG

signals were triggered by the FR events in the out-node. Displayed are non-propagating FR events (n=138) in the out-node (A1) and the in-node (A2), and propagating FR events (n=47) in the out-node (A3) and the in-node (A4) in an SOZ:SOZ edge patient 4145. (B) Example average fitting oscillations & one over f (fooof) derivations for the non-propagating out- (B1) and in-node (B2) iEEG signals, and propagating out-node (B3) and in-node (B4) iEEG signals corresponding to those used to derive A1-4. Blue line indicates aperiodic fit, red line indicates full model fit (C,D). Another example of FR propagation in another edge in patient 4145 displayed as in A,B with n=156 non-propagating FR, and n=251 propagating FR. Note that in A,B and C,D, propagated FR in the out- node were associated with a more time-locked triggered epileptiform spike that was also quantified by an increase in the aperiodic offset, as compared to non-propagated FR. In individual traces FR onset always preceded the onset of the negative component of the epileptiform spike (E-F). Summary plot of comparisons of derived average fooof parameters calculated between the non-propagating events (np) and propagating (p) events in the out-node (E) and in-node (F) in the 29 soz:soz edges of 6 patients shown in distinct colors. Asterisk next to the plot title indicates statistical significance (paired t-test, p-adjusted<0.05).

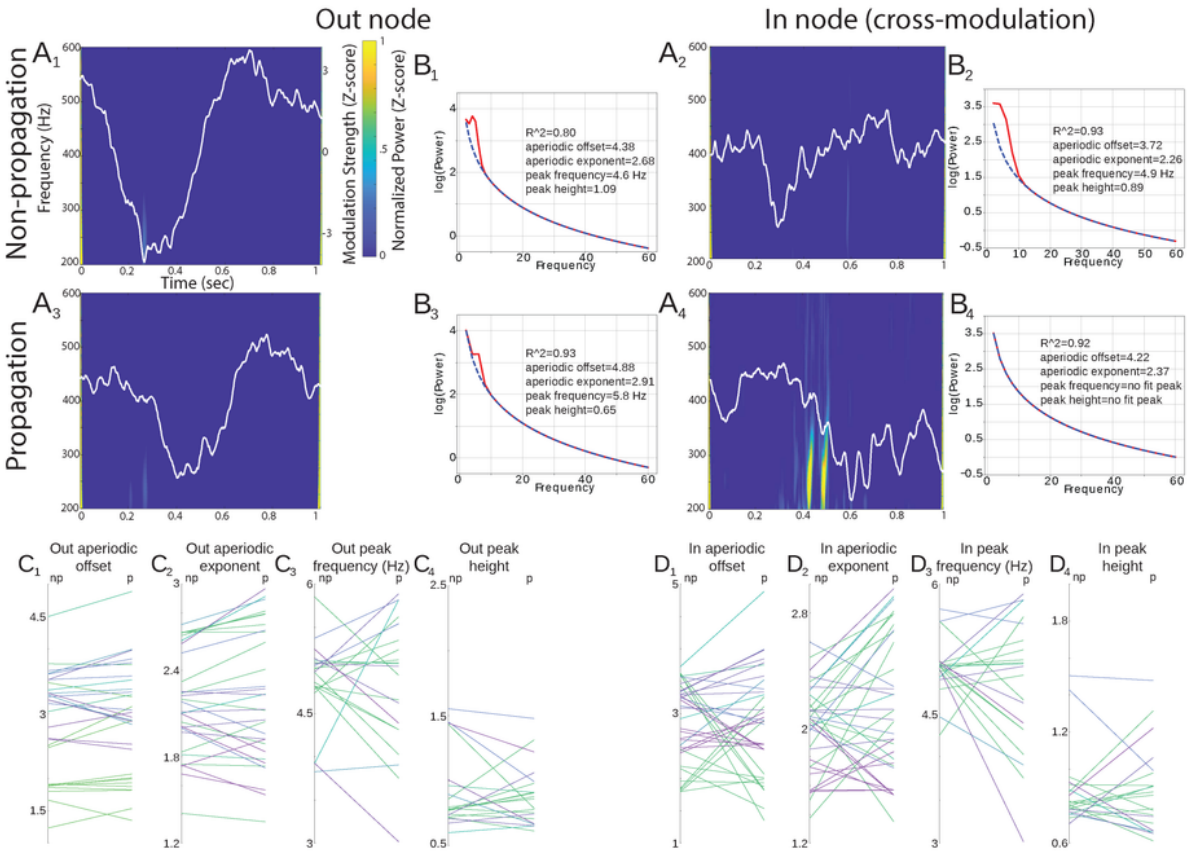

Figure 5

Fast ripple (FR) propagation in the non-seizure onset zone (NSOZ) is associated with heterogenous changes in the intracranial EEG (iEEG). (A) Example FR triggered average of iEEG signals (white traces). The peak-to-peak amplitude corresponds to the strength of modulation with FR events that are temporally aligned, with onset at 250 ms, and modulated as shown by the normalized averaged time-frequency representation. To demonstrate cross-modulation, the in-node averaged iEEG signals were triggered by

the FR events in the out-node. Displayed are non-propagating FR events (n=110) in the out-node (A1) and the in-node (A2), and propagating FR events (n=11) in the out-node (A3) and the in-node (A4) in an NSOZ:NSOZ edge patient IO018. (B) Example average fitting oscillations & one over f (fooof) derivations for the non-propagating out- (B1) and in-node (B2) iEEG signals, and propagating out-node (B3) and in-node (B4) iEEG signals that correspond to those used to derive A1-4. Blue line indicates aperiodic fit, red line indicates full model fit. (C-D) Summary plot of comparisons of derived average fooof parameters calculated between the non-propagating events (np) and propagating (p) events in the out node (E) and in node (F) in the 35 soz:nsoz, nsoz:soz, and nsoz:nsoz edges of 8 patients shown in distinct colors. None of the comparisons were statistically significant (paired t-test, p-adjusted>0.05).

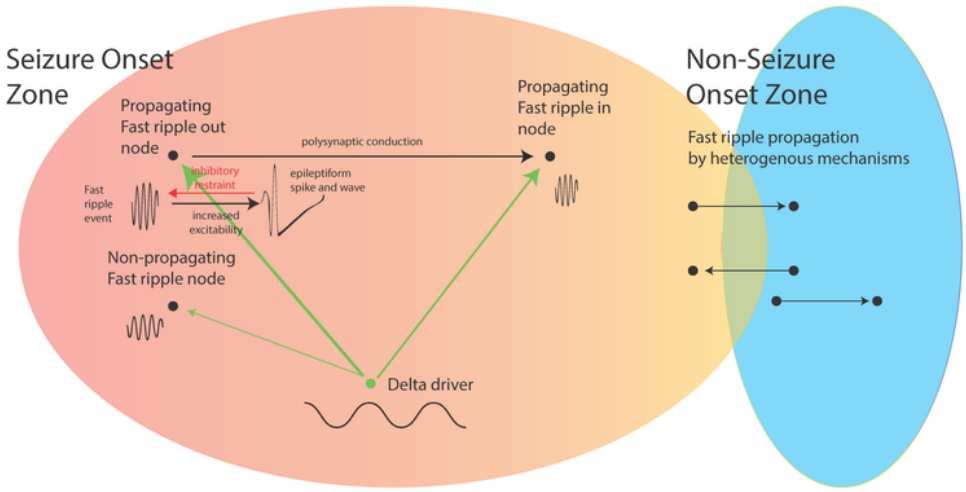

Figure 6

Graphical illutration of the mechanisms of fast ripple (FR) propagation. In the seizure onset zone, FR generating nodes receive inputs from delta oscillation drivers (green circle). The strength of coupling between delta and FR events is shown by the thickness of the green arrow. The FR occur near or at the peak of the delta oscillation. The two nodes (black circles) with FR propagation across the connecting edge (black line) exhibit stronger FR-delta coupling at the out- and in-node as compared with the node

with non-propagating FR. At the out-node with FR propagation, the propagated FR is higher power and higher frequency as compared with a non-propagated FR. At the out-node a propagated FR event precedes an epileptiform discharge likely through increased neuronal excitability overcoming an inhibitory restraint mechanism. The propagated FR event at the out-node reaches the in-node at a relatively slow velocity through poly-synaptic conduction. At the in-node the FR is relatively lower in power and higher in frequency. FR propagation in NSOZ:SOZ, SOZ:NSOZ, and NSOZ:NSOZ edges involves diverse unresolved mechanisms.

Supplementary Files

This is a list of supplementary files associated with this preprint. Click to download.

- supplementalmaterials.pdf